Acta Crystallographica Section D
Biological Crystallography
ISSN 0907-4449

Analysis of quinazoline and pyrido[2,3-*d*]-pyrimidine N9—C10 reversed-bridge antifolates in complex with NADP$^+$ and *Pneumocystis carinii* dihydrofolate reductase

Vivian Cody,[a]* Nikolai Galitsky,[a] Joseph R. Luft,[a] Walter Pangborn,[a] Sherry F. Queener[b] and Aleem Gangjee[c]

[a]Hauptman–Woodward Medical Research Institute, Inc., 73 High Street, Buffalo, NY 14203, USA, [b]Department of Pharmacology and Toxicology, Indiana University School of Medicine, Indianapolis, IN 46202, USA, and [c]Division of Medicinal Chemistry, Graduate School of Pharmaceutical Sciences, Duquesne University, Pittsburgh, PA 15282, USA

Correspondence e-mail: cody@hwi.buffalo.edu

Received 28 January 2002
Accepted 11 June 2002

PDB References: 2,4-diamino-6-[*N*-(2′,5′-dimethoxybenzyl)-*N*-methylamino]quinazoline–NADP$^+$–DHFR complex, 1ly3, r1ly3sf; 3′,5′-dimethoxypyrido[2,3-*d*]pyrimidine–NADP$^+$–DHFR complex, 1ly4, r1ly4sf.

Structural studies of two ternary complexes of *Pneumocystis carinii* dihydrofolate reductase (*pc*DHFR) with the cofactor NADP$^+$ and potent antifolates, the N9—C10 reversed-bridge inhibitor 2,4-diamino-6-[*N*-(2′,5′-dimethoxybenzyl)-*N*-methylamino]quinazoline (1) and its 3′,5′-dimethoxypyrido[2,3-*d*]pyrimidine analog (2), were carried out. Data for the monoclinic crystals were refined to 1.90 Å resolution for the complex with (1) (R = 0.178) and to 2.1 Å resolution for the complex with (2) (R = 0.193). The effect of the N9—C10 reversed-bridge geometry is to distort the bridge from coplanarity with the pyrido[2,3-*d*]pyrimidine or quinazoline ring system and to twist the C10 methylene conformation toward a *gauche* conformation. This change also influences the conformation of the methoxybenzyl ring, moving it away from a *trans* position. This change places the 5′-methoxy group deeper within the hydrophobic pocket made by Ile65, Pro66 and Phe69 of the *pc*DHFR active site. These results also revealed the first observation of an unusual conformation for the reversed-bridge geometry (C5—C6—N9—C10 torsion angle) in antifolate (2). The electron density is consistent with the presence of two models (conformers 2-1 and 2-2) that result from inversion of the geometry at N9. The four examples of N9—C10 reversed-bridge antifolates cluster in two conformations, with the structure of quinazoline (1) similar to that previously reported for its 2′,5′-dimethoxypyrido[2,3-*d*]pyrimidine analog (3). The two conformers of (2) differ from these and each other by a twisted-bridge geometry that results in the dimethoxybenzyl ring occupying the same conformational space. Conformer 2-2 also has the N9—C10 reversed bridge perpendicular to the pyrido[2,3-*d*]pyrimidine plane, in contrast to the *gauche–trans* conformation normally observed. As a result of these changes, the N9 methyl probes conformational space in the active site not normally occupied by antifolate structures. The N9 methyl of conformer 2-2 makes close contacts to the conserved Leu25 as well as the hydroxyl O atoms of the nicotinamide ribose and Ser64, whereas the other three reversed-bridge conformers make weak hydrophobic contacts with Ile123, Thr61 and Ile65. These antifolates are ten times more selective for *pc*DHFR than the C9—N10 bridge parent trimetrexate. However, pyrido[2,3-*d*]pyrimidines (2) and (3) are three times more selective for *pc*DHFR than quinazoline (1) is for rat liver DHFR. These data suggest that the loss of hydrogen-bonding interactions with N8 is more important to potency than the interactions of the methoxybenzyl substituents.

1. Introduction

Infections with *Pneumocystis carinii* (*pc*) and *Toxoplasma gondii* (*tg*) are still major causes of death in patients with immune-compromised conditions, in particular those with

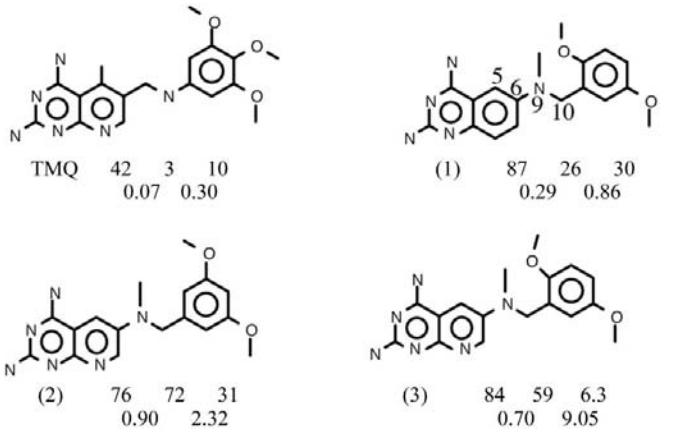

Figure 1
Schematic representation of N9—C10 reversed-bridge analogs (1), (2) and (3), and TMQ, the parent compound. Also listed are the biological activity data as reported in Gangjee *et al.* (1998). The first line gives IC_{50} (μM) for *P. carinii*, rat liver (rl) and *T. gondii* DHFR, respectively. The second line is the selectivity ratio of IC_{50} for rl/*pc* and rl/*tg*.

AIDS (Mills & Masur, 1990). Antifolates have been shown to be effective against dihydrofolate reductase (DHFR) from the *pc* and *tg* pathogens and are therefore of interest as targets for drug-design studies. Recently, trimetrexate (TMQ; Fig. 1) has been approved for treatment of *pc* infections (Masur *et al.*, 1993). Biological data for a series of quinazolines revealed that the removal of the 5-methyl substituent enhanced their inhibitory potency against human DHFR (Gangjee *et al.*, 1998). Further modification of this series to include a N9—C10 reversed bridge and a variable benzyl methoxy-substitution pattern showed that these analogs had even greater potency against *pc*DHFR and *tg*DHFR (Gangjee *et al.*, 1998). These results are in contrast to data for a similar series of pyrido[2,3-*d*]pyrimidines with N9 methylation that showed decreased inhibitory potency against *tg*DHFR (Gangjee *et al.*, 1996). Furthermore, those quinazoline analogs with a 2′,5′- or 3′,5′-dimethoxy-substituted benzyl ring were more potent for fungal DHFR than those with 3′,4′,5′-trimethyoxy substitutions (Fig. 1; Gangjee *et al.*, 1996). As illustrated (Fig. 1), the 2′,5′-dimethoxyquinazoline (1) is three times less selective for *pc*DHFR than either the 3′,5′- or 2′,5′-dimethoxypyrido-[2,3-*d*]pyrimidines (2) and (3). This selectivity pattern differs for *tg*DHFR in that (3) is ten times more selective for *tg*DHFR than the corresponding quinazoline (1). One rationale for the synthesis of 5-desmethyl analogs was to decrease their inhibitory potency for mammalian DHFR and to increase their selectivity for the pathogenic enzymes.

Sequence alignment of the DHFR from human (hDHFR), *pc* and *tg* indicate that there are several highly conserved residues among them and that the active-site regions are homologous (Roos, 1993). The most significant difference among these three enzymes is that the acidic active-site residue 32 (*pc* numbering) is Glu in hDHFR and *pc*DHFR, but is Asp in *tg*DHFR (Table 1). Although the hydrophobic character at positions 33 and 65 is conserved, there are residue changes. One of the more dramatic changes involves position 37 (Gln, Lys, Ser). Structural data reveal that there is sub-domain movement of the loop involving residue 37 toward the conserved Arg75 when the inhibitor does not contain a *p*-aminobenzylglutamate moiety. The strength of the hydrogen-bonding interactions between residue 37 and the conserved Arg75 would be affected by the residue changes among these DHFR enzymes that could affect the selectivity of enzyme inhibition.

To understand this pattern of potency and selectivity for *pc*DHFR and *tg*DHFR, crystallographic results are reported for two inhibitor–$NADP^+$ cofactor ternary complexes with *pc*DHFR and the 2′,5′-dimethoxy N9-methyl quinazoline

Table 1
Sequence comparison among DHFR.

Residue (*pc* numbering)	hDHFR	*pc*DHFR	*tg*DHFR
32	Glu	Glu	Asp
33	Phe	Ile	Phe
35	Tyr	Tyr	His
37	Gln	Lys	Ser
65	Ile	Ile	Met
69	Asn	Phe	Phe

Table 2
Crystal properties and refinement statistics.

Crystal properties.

Properties	*pc*DHFR–$NADP^+$–(1)	*pc*DHFR–$NADP^+$–(2)
Unit-cell parameters		
a (Å)	37.33	37.05
b (Å)	43.26	43.13
c (Å)	61.37	60.73
β (°)	94.77	94.60
Space group	$P2_1$	$P2_1$
Resolution range (Å)	8.0–1.90	8.0–2.1
R_{merge} (%)	4.3	6.6
Completeness (last shell) (%)	51.0	69.1
Overall completeness (%)	88.3	94.2
No. of reflections used	11539	8544
Total No. of reflections	13784	10692
R factor (%)	17.8	19.3
No. of protein atoms	1686	1678
No. of water molecules	76	32
Ramachandran plot, most favored (*PROCHECK*) (%)	88.1	83.2
B factor (protein average) (Å^2)	25.67	30.21

Refinement statistics.

	R.m.s. σ	Target σ	R.m.s. σ
Distances (Å)			
Bonds	0.018	0.020	0.020
Angles	0.048	0.040	0.063
Planar 1–4	0.055	0.050	0.062
Planar groups	0.014	0.025	0.022
Chiral volume	0.171	0.500	0.228
Single torsion	0.205	0.500	0.245
Multiple torsion	0.275	0.500	0.339
Possible hydrogen bonds	0.238	0.500	0.310
Torsion angles (°)			
Planar	2.4	3.0	3.4
Staggered	20.4	15.0	25.3
Orthonormal	24.9	15.0	25.8

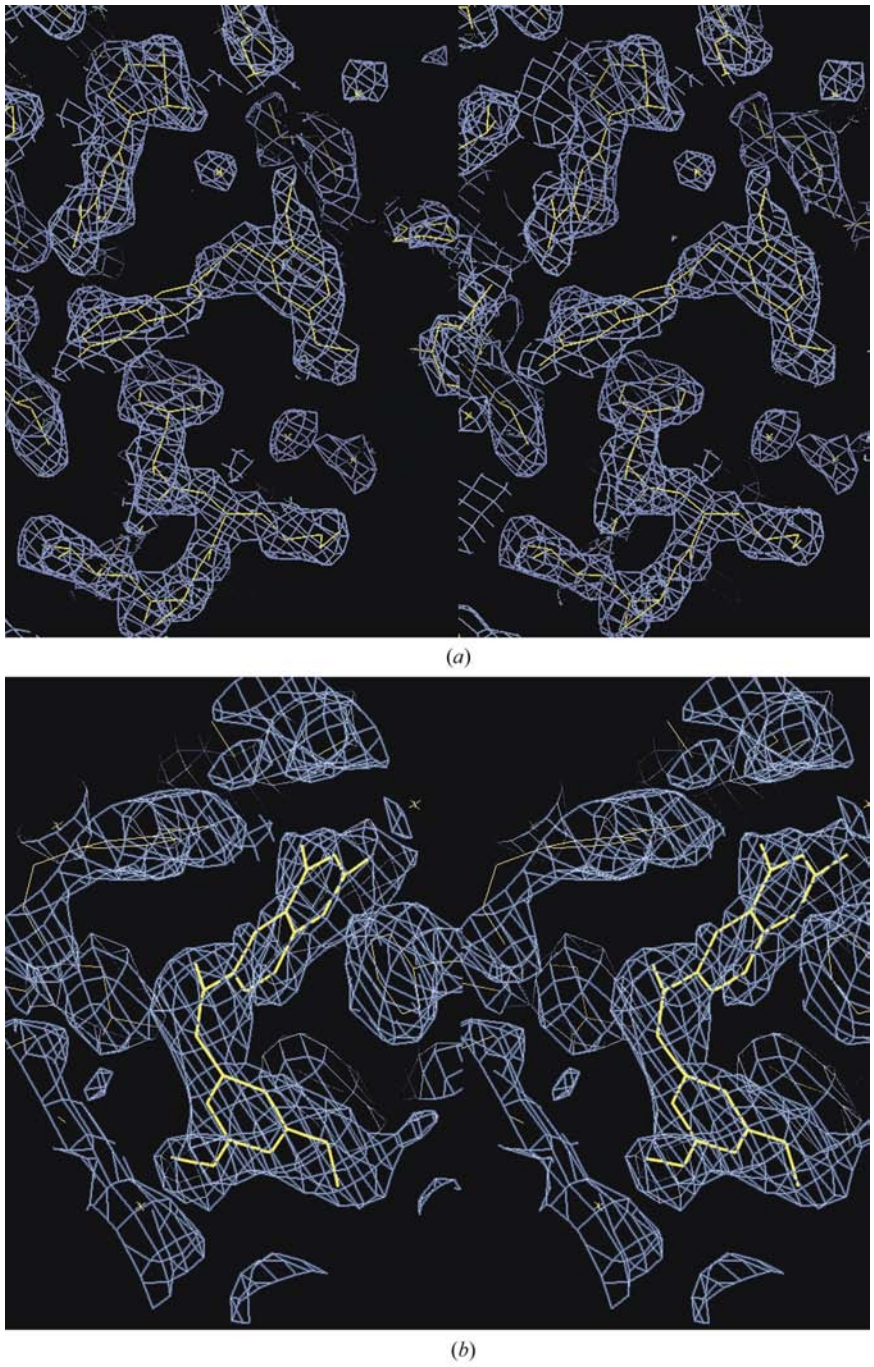

Figure 2
(*a*) Stereoview of $2F_o - F_c$ electron density (blue), using phases calculated from only the protein, in *pc*DHFR–NADP$^+$–(1) showing the fit of the enzyme, inhibitor and cofactor (yellow) to the density. (*b*) Stereoview of $2F_o - F_c$ electron-density map (blue), using phases calculated from only the protein, in *pc*DHFR–NADP$^+$–(2) showing the fit of the enzyme, inhibitor and cofactor (yellow) to the density. The diagrams were produced with *CHAIN* (Sack, 1988).

pyrido[2,3-*d*]pyrimidine (1) and its 3′,5′-dimethoxy quinazoline analog (2) (Fig. 1). These data are compared with the previously reported structural complex for the F31G variant of hDHFR with the 2′,5′-dimethoxy pyrido[2,3-*d*]pyrimidine analog (3) (Gangjee *et al.*, 1998).

2. Experimental

2.1. Crystallization and X-ray data collection

Recombinant *pc*DHFR was isolated and purified as previously described (Broughton & Queener, 1991). The protein was washed in a Centricon-10 three times with 50 m*M* MES buffer at pH 6.0 in 100 m*M* KCl buffer and concentrated to 8.6 mg ml^{-1} for (1) and 12.8 mg ml^{-1} for (2). A novel thermal gradient technique (Luft *et al.*, 1999*a*,*b*) was used to carry out crystallization screens with *pc*DHFR. Crystallization of the *pc*DHFR–(1) complex was carried out by adding 2.5 µl of protein, 1.5 µl of MES–KCl buffer and 7 µl of 50%(*w*/*v*) PEG 2000 in 50 m*M* MES pH 6.0, 100 m*M* KCl for (1) and adding 10 µl of protein, 5 µl of MES–KCl buffer and 5 µl of 50%(*w*/*v*) PEG 2000 in 50 m*M* MES pH 6.0, 100 m*M* KCl for (2). These solutions were placed in microcentrifuge tubes for equilibration on a thermal gradient apparatus. Samples of *pc*DHFR were also incubated with NADP$^+$ along with (1) or (2) and incubated overnight at 277 K.

Data collection was carried out at room temperature on the best crystals available using a Rigaku R-AXIS IV imaging-plate system with a rotating-anode source and processed using *DENZO* (Otwinoski & Minor, 1997). Crystal lattice properties and data-collection statistics are listed in Table 2.

2.2. Structure determination and refinement

The structures of the *pc*DHFR–NADP$^+$–(1) and *pc*DHFR–NADP$^+$–(2) complexes were solved by molecular-replacement methods with the restrained least-squares program *PROLSQ* (Hendrickson & Konnert, 1980; Finzel, 1987) in combination with the model-building program *CHAIN* (Sack, 1988). All calculations were carried out on a Silicon Graphics Impact R10000 workstation. The initial $(2|F_o| - |F_c|)\exp(i\alpha c)$ maps, where F_o are the observed and F_c the calculated structure factors based on the protein model only and αc is the calculated phase, resulted in electron density corresponding to both the inhibitors (1) and (2) and the cofactor, NADP$^+$, as well as a good fit of the protein to its density (Fig. 2).

Further restrained refinement was continued for the ternary complex, including the cofactor and inhibitor. Models of (1)

and (2) were generated from the crystal structure of (3) (Gangjee *et al.*, 1998) and optimized with *SYBYL* (Tripos Inc., 1997). The aromatic rings of the inhibitors and $NADP^+$ were constrained to be planar. Between least-squares minimizations, the structure was manually adjusted to fit difference electron density and verified by a series of OMIT maps calculated from the current model with deleted fragments. The final refinement statistics are summarized in Table 2. The Ramachandran conformational parameters from the last cycle of refinement generated by *PROCHECK* (Laskowski *et al.*, 1993) show that between 88 and 83% of the residues have the most favored conformation and none are in disallowed regions for complexes (1) and (2), respectively.

3. Results

3.1. Overall structure

The overall characteristics of these *pc*DHFR complexes are similar to those reported previously (Cody *et al.*, 1993, 1997, 1999; Champness *et al.*, 1994), in particular the folate–$NADP^+$–*pc*DHFR ternary complex (Fig. 3). These data have similar conformations near the flexible loops 23 and 47 as the folate complex (Cody *et al.*, 1999). There is a slight shift in the position of the *C* helix (residues 60–65) compared with that observed for the other *pc*DHFR complexes (maximum of 0.8 Å) between the α carbon of Ile65 of complexes for *pc*DHFR–$NADP^+$–(1) and *pc*DHFR–$NADP^+$–(2).

These data also provide the first structural observation of an N9—C10 reversed-bridge antifolate bound to *pc*DHFR. Structural details for a hybrid molecule, containing key features of the lipophilic antifolates TMQ, were previously reported for the 2′,5′-dimethoxy analog (3) and NADPH with hDHFR (Gangjee *et al.*, 1998). The binding orientation of the pyrido[2,3-*d*]pyrimidine or quinazoline ring in these *pc*DHFR complexes is similar to those observed in other *pc*DHFR complexes (Cody *et al.*, 1993, 1997, 1999; Champness *et al.*, 1994). The overall pattern of intermolecular contacts is shown in Table 3.

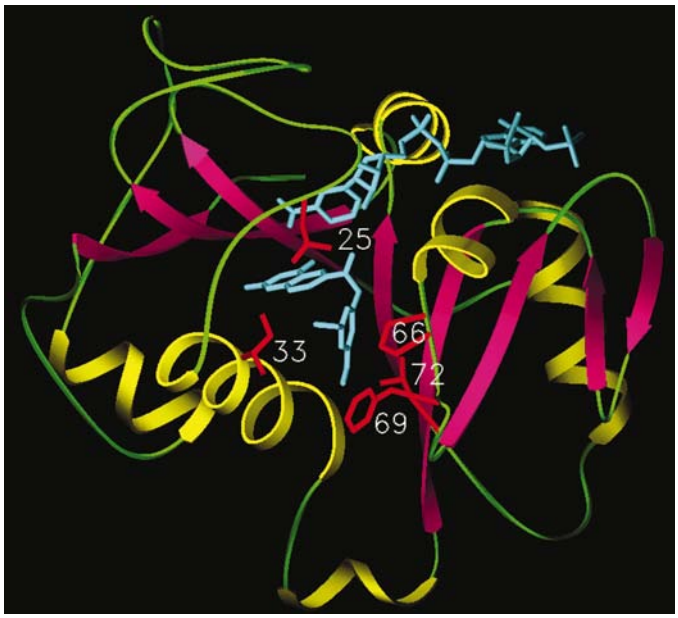

Figure 3
Model of the tertiary structure of the *pc*DHFR–$NADP^+$–(2) ternary complex. Helices are in yellow, sheets are in red and loops are in green. Active-site hydrophobic residues Leu25, Ile33, Pro66, Phe69 and Ile72 are shown. Models were produced with *SETOR* (Evans, 1993).

Table 3
Inhibitor and cofactor intermolecular contacts (°) in hDHFR and *pc*DHFR complexes.

Contacts (Å)	*pc*DHFR–(1)	*pc*DHFR–(2)	hDHFR–(3)†	*pc*DHFR–MTX‡
4 NH2···Ile10 O	3.0	2.7	3.0	2.5
4 NH2···Tyr129 OH	3.4	3.2	3.5	3.3
4 NH2···nic O	3.7	3.4	3.6	3.6
4 NH2···Val123 O	2.7	3.3	3.1	3.0
2 NH2···water	3.5	—	3.2	3.2
2 NH2···Glu32 OE2	2.7	2.9	2.7	2.9
N1···Glu32 OE1	2.8	2.8	3.0	2.6
Glu32 OE1···water	2.9	3.4	—	2.4
Glu32 OE2···Thr144 Oγ	2.7	2.6	2.7	3.2
Thr144 Oγ···water	2.8	—	2.8	—
Arg75 NH1···water	2.9	—	—	3.3
Arg75 NH2···water	3.7	—	3.5	—
Arg75 NH2···Lys73 O	3.0	2.8	3.1	2.6
Arg75 NH1···Thr40 Oγ	3.1	2.4	2.7	3.5
Trp27 NE1···water	3.3	2.5	—	3.2
Water···Glu32 OE1	2.5	3.6	—	2.4
N8···water	3.1	—	—	2.8
N8···Glu32 OE1	3.7	3.4	3.7	2.8

† Gangjee *et al.* (1998). ‡ Cody *et al.* (1999).

3.2. Inhibitor binding

The carboxylate O atoms of Glu32 in both inhibitor complexes interact with the diamino ring system and forms contacts with the N1 N atom by OE2 and OE1 to the 2-amino group (Table 3). In addition, the carboxylate OE1 of Glu32 forms a hydrogen bond to the hydroxyl group of the conserved Thr144, which in turn interacts with a conserved water molecule reported in most DHFR structures (Cody *et al.*, 1993, 1997, 1999; Champness *et al.*, 1994). In the case of the complex with (2), this water was not observed in the electron-density map. Similarly, there is an interaction of the Glu32 OE2 with a conserved water that in turn forms contacts with the conserved Trp27 and to the pyrido[2,3-*d*]pyrimidine N8 of (2). Another difference between the interactions of the *pc*DHFR complexes of (1) and (2) is that no water was observed in the channel that interacts with the conserved Arg75, as was observed in *pc*DHFR–(1) and *pc*DHFR–MTX (Cody *et al.*, 1999) complexes. There is also a change in the conformation of Lys73 and Thr40 in these complexes, which form hydrogen bonds to Arg75 that are not present in the *pc*DHFR–MTX complex (Table 3).

Comparison of the *pc*DHFR complexes with inhibitors (1) and (2) reveals the first observation of an unusual conformation of the N9—C10 reversed bridge (Table 4). The conformation of inhibitor (1) differs from that previously reported for the hDHFR complex with inhibitor (3) (Gangjee *et al.*,

1998) and from TMQ, which has a normal C9—N10 bridge (Cody *et al.*, 1993). The data for the structure of the *pc*DHFR complex with (2) indicate that two alternate conformers are present in equal populations, as the electron density for the inhibitor is consistent with the presence of two models that result from inversion of the geometry at N9 (Fig. 4). Both conformers of (2) (2-1 and 2-2) differ from either the *pc*DHFR–(1) or hDHFR–(3) complexes (Table 4). The most significant change among these four reverse-bridged examples is observed for the C5—C6—N9—C10 torsion angle in the second conformer 2-2 of the 3′,5′-dimethoxy TMQ analog (2) which places the N9—C10 bridge perpendicular to the pyrido[2,3-*d*]pyrimidine plane. The sum of these permutations in the bridge conformation of (2) results in the dimethoxybenzyl ring occupying the same conformational space within the active site (Fig. 5). These data show that the 5′-methoxy group of all four reversed-bridge analogs makes close contacts to Phe69 and Leu72 in the *pc*DHFR structures, and to Leu67 and Gln35 in the human structure (Fig. 6). The contacts are shorter in the hDHFR complex. On the other hand, the 2′-methoxy group makes weaker contacts to Leu25 and Ser65 in *pc*DHFR and only to Leu22 in hDHFR. In the complex with (2), the 3′-methoxy makes intermolecular contacts with Leu25, Ile33 and Pro66.

The N9 methyl of these reversed-bridge antifolates probes different regions of the active site as a consequence of changes in the bridge geometry. For example (Fig. 6), in inhibitors (1) and (3) the N9 methyl makes contact with residues Thr61, Ile65 and the nicotinamide ring, whereas that in the alternate conformer 2-1 makes close contacts to Thr61, while maintaining similar contacts to Ile65, Ile123 and the nicotinamide ring. On the other hand, that in conformer 2-2 makes close contacts with Leu25, as well as the hydroxyl groups of the nicotinamide ribose and Ser64.

3.3. NADP$^+$ binding

Although the cofactor NADP$^+$ is bound in an extended conformation similar to other *pc*DHFR–cofactor complexes (Cody *et al.*, 1997, 1999; Champness *et al.*, 1994) (Table 5), there is variation in the conformation of the nicotinamide-ribose and pyrophosphate moieties (*i.e.* θ_n and ψ_n; Table 6). The conformation of the nicotinamide-ribose group in these complexes more closely resembles that observed in the MTX ternary *pc*DHFR complex than the folate *pc*DHFR complex. However, the pyrophosphate-bridge conformation shows greater variation in these complexes than either the MTX or FA complexes (Cody *et al.*, 1999).

The carboxamide group of the nicotinamide ring, which is *syn* to the nicotinamide ring N, makes a series of strong hydrogen bonds with conserved residues Ala12 and Ile19 in *pc*DHFR (Table 5). These contacts for (1) and (2) are stronger than those observed in the MTX–*pc*DHFR ternary complex (Cody *et al.*, 1999). The conserved *cis*-peptide linkage between the invariant Gly124 and Gly125 permits interaction with the pyrophosphate O atoms that are positioned at the end of the

Table 4
NADP$^+$ contacts (Å) in *pc*DHFR–inhibitor complexes.

	(1)	(2)	MTX†
Nic carboxamide			
O···4 NH2	3.7	3.4	2.7
O···Ala12 N	3.0	3.1	3.6
O···Tyr129 OH	3.6	3.9	2.9
N···Ala12 O	2.6	2.4	2.8
N···Ile19 O	2.9	2.9	3.2
Ile10 O···Tyr129 OH	2.8	2.5	2.7
Nic ribose			
O1···water	2.8	—	—
O1···Ser64 Oγ	4.2	2.9	4.2
O2···water	3.1	2.8	—
O2···Ser24 N	3.3	—	—
Pyrophosphate			
O5···Gln127 N	3.1	3.0	2.8
O6···water	2.8	—	—
O15···Thr61 N	3.0	3.1	3.0
O16···Gly125 N	3.2	3.3	3.0
Adenine			
5 NH2···water	3.1	2.9	3.2
3′-Phosphate			
O11···Arg82 N	2.6	3.1	3.7
O12··· Thr81 Oγ	2.8	—	—
O13··· Arg59 NH1	3.7	2.8	2.3
N nic···5 NH2	17.5	17.7	16.4

† Cody *et al.* (1999).

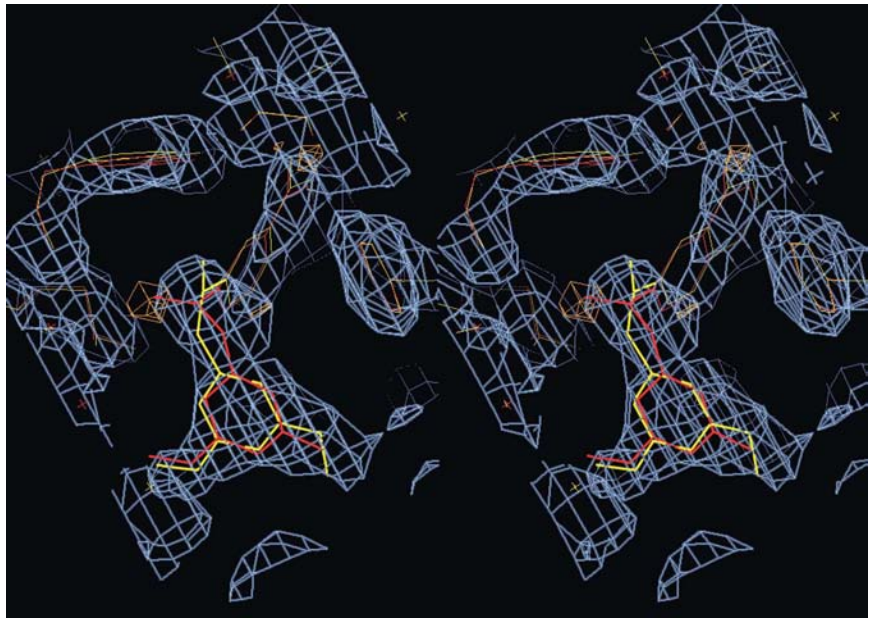

Figure 4
Stereoview of the electron density ($2F_o - F_c$, 1σ) (blue) and ($F_o - F_c$, -3σ) (red) that results from phases of conformer 1 only, showing the fit of the inhibitor (2) in conformation 1 (red) and conformation 2 (yellow) in *pc*DHFR–NADP$^+$ ternary complex. Diagram produced with *CHAIN* (Sack, 1988).

central helix *C*. The largest changes in the NADP$^+$ conformation also occur at this position (Table 6).

The nicotinamide-ribose hydroxyl O1 interacts with a water molecule in (1) that is not observed in the structures of (2) or MTX (Cody *et al.*, 1999) (Table 6). O1 also makes a close contact in (2) with the hydroxyl of Ser64 that is not observed in (1) or MTX, indicating a change in the conformation of Ser64 in this structure. The pyrophosphate O atoms make a series of close contacts with the backbone N atoms of Gln127, Thr61 and Gly125 that are conserved in all structures (Table 6).

The most notable differences in the NADP$^+$ contacts in these complexes are those involving the 3′-phosphate. Also, as indicated (Table 5), the overall conformation of NADP$^+$ is more extended in complex with (2) than observed for the MTX–*pc*DHFR ternary complex (Cody *et al.*, 1999).

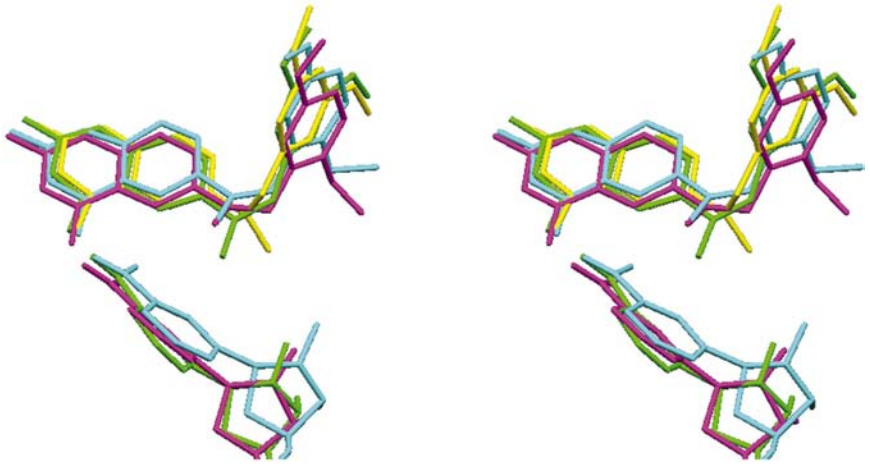

Figure 5
Stereoview showing the overlap of the four examples of N9—C10 reversed-bridge antifolates (1) (magenta), (2) (green and yellow) and (3) (cyan). The nicotinamide ring of the cofactor NADP$^+$ is also also shown. Models produced with *SETOR* (Evans, 1993).

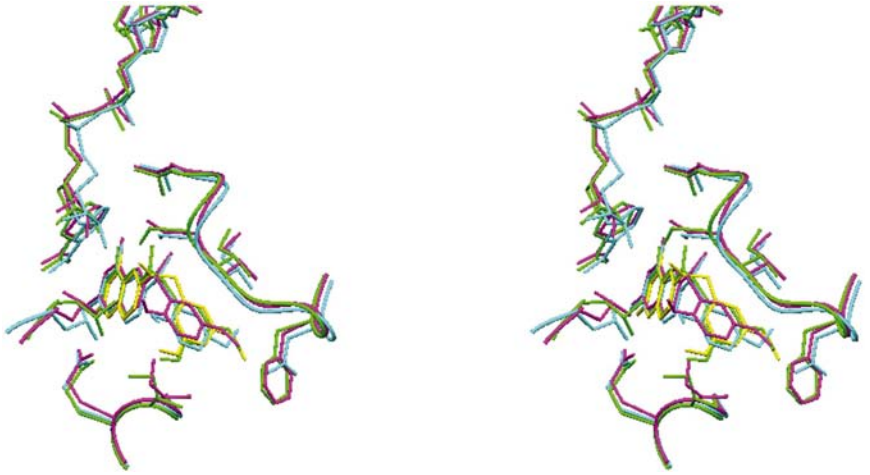

Figure 6
Stereoview of the four examples of N9—C10 reversed-bridge antifolates (1) (magenta), (2) (green and yellow) and (3) (cyan), highlighting their interactions in the active site of either *pc*DHFR or hDHFR. The active-site residues Leu25/22, Glu32/30, Ile33/Phe31, Thr61/56, Ser64/59, Ile65/60 and Phe69/Asn64 and the cofactor NADP$^+$ are shown for *pc* and h sequences, respectively. Models produced with *SETOR* (Evans, 1993).

4. Discussion

This is the first observation of an unusual N9—C10 reversed-bridge conformation for the 3′,5′-dimethoxy TMQ analog (2) in the *pc*DHFR ternary complex. This novel conformation is a result of inversion at the N9 position. The flexibility in the bridge conformation places the 5′-methoxy group deep within the hydrophobic pocket made by Ile65, Pro66 and Phe69 of the *pc*DHFR active site. In the human enzyme, these residues are Ile60, Pro61 and Asn64, thereby changing the nature of the intermolecular contacts. The 3′-methoxy group makes less favorable contacts than the 5′-methoxy with the active-site surface and interacts with Leu25, Ile33 and Pro66. In the human structure, these residues are Leu22, Gly31 and Pro61. The mutation of Phe31 to Gly in the F31G-hDHFR–NADPH–(3) ternary complex provides a greater conformational space for the 2′,5′-dimethoxybenzyl ring compared with the *pc*DHFR complexes.

The overall effect of the N9—C10 reversed-bridge geometry is to distort the bridge from coplanarity with the pyrido[2,3-*d*]pyrimidine or quinazoline ring system and to twist the C10 methylene conformation towards a *gauche* conformation. This change also influences the conformation of the methoxybenzyl ring, moving it away from a *trans* position. When the two alternate conformers of inhibitor (2) are compared (Fig. 4), it is seen that the changes in bridge conformation take place in a concerted manner that places the 3′,5′-methoxy groups in the same conformational space. The 5′-methyl of inhibitors (1) and (2) makes a van der Waals contact with Phe69 in both structures, while the 2′-methyl group in (1) interacts with Ile33. In hDHFR, there are two sequence changes at these interaction sites, Asn64 and Phe31. Since the hDHFR complex is with a Gly31 mutant, there are no contacts made to the 2′-methoxy group of (3).

These data support the hypothesis that the N9—C10 reversed-bridge analogs of TMQ have decreased potency and increased selectivity for *pc*DHFR, with the greatest *pc* selectivity shown for the 3′,5′-dimethoxy TMQ analog (2) (Fig. 1), which is a result of optimal placement of the methoxy groups in the hydrophobic pocket of the active site. In the case of *pc*DHFR, these contacts are more favorable because of the Phe69 substitution compared with the Asn64 in the hDHFR sequence.

The decreased selectivity of the quinazoline analog (1) is the result of changes in bridge conformation, coupled with differ-

Table 5
N9—C10 reversed-bridge torsion angles in DHFR complexes.

Structures	C5—C6—N9—C10	C6—N9—C10—C11	N9—C10—C11—C12	C5—C6—N9—CH3
hDHFR–TMQ† (°)	169.1	86.1	175.9	—
F31G-hDHFR–(3)‡ (°)	170.6	53.3	−138.2	−24.6
*pc*DHFR–(1)	147.4	77.7	−153.4	−30.8
*pc*DHFR–(2), conf. 1	−153.9	21.9	−116.9	−0.2
*pc*DHFR–(2), conf. 2	−90.9	−71.4	−38.9	92.4

† Cody *et al.* (1993). ‡ Gangjee *et al.* (1998).

Table 6
Cofactor (NADPH or $NADP^+$) conformation in *pc*DHFR ternary complexes.

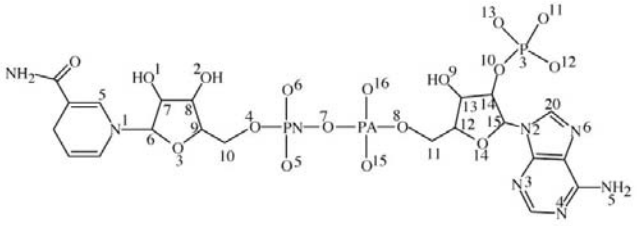

	Torsion angle	Inhibitor (1)	(2)	MTX†	FA†
χ_n	C5—N1—C6—C7	125.9	118.0	128.2	119.3
ξ_n	C8—C9—C10—O4	−171.2	170.5	−168.3	−178.4
θ_n	C9—C10—O4—P_n‡	142.6	149.8	165.7	123.7
ψ_n	C10—O4—P_n—O7	58.3	49.7	59.3	67.3
φ_n	O4—P_n—O7—P_a‡	87.9	82.8	105.9	58.9
φ_a	P_n—O7—P_a—O8	141.8	159.9	118.6	176.4
ψ_a	O7—P_a—O8—C11	−84.4	−76.2	−77.6	−61.5
θ_a	P_a—O8—C11—C12	−155.1	−143.9	−152.8	−149.5
ξ_a	O8—C11—C12—C13	179.1	171.2	−170.9	164.6
χ_a	C14—C15—N2—C20	−120.5	−111.2	−122.7	−114.8
θ'_a	C15—C14—O10—P3	164.1	158.1	163.4	162.8

† Cody *et al.* (1999). ‡ Subscript *n*, torsion angles for nicotinamide nucleoside; subscript *a*, torsion angles for adenine nucleoside.

ences in basicity of the quinazoline ring system and the lack of a hydrogen-bonding interaction that is normally observed between a structural water and the N8 of the pteridine or pyrido[2,3-*d*]pyrimidine ring system.

This work was supported by NIH grants GM-51670 (VC), AI47759 (AG) and AI4461 (AG).

References

Broughton, M. C. & Queener, S. F. (1991). *Antimicrob. Agents Chemother.* **35**, 1348–1355.
Champness, J. N., Achari, A., Ballantine, S. P., Byrant, P. K., Delves, C. J. & Stammers, D. K. (1994). *Structure*, **2**, 915–924.
Cody, V., Galitsky, N., Luft, J. R., Pangborn, W., Gangjee, A., Devraj, R., Queener, S. F. & Blakely, R. L. (1997). *Acta Cryst.* D**53**, 638–649.
Cody, V., Galitsky, N., Rak, D., Luft, J. R., Pangborn, W. & Queener, S. F. (1999). *Biochemistry*, **38**, 4303–4312.
Cody, V., Wojtczak, A., Kalman, T. I., Freisheim, J. H. & Blakley, R. L. (1993). *Adv. Exp. Biol. Med.* 481–486.
Evans, S. V. (1993). *J. Mol. Graph.* **11**, 134–138.
Finzel, B. C. (1987). *J. Appl. Cryst.* **20,** 53–55.
Gangjee, A., Vasudevan, A., Queener, S. F. & Kisliuk, R. L. (1996). *J. Med. Chem.* **39**, 1438–1446.
Gangjee, A., Vidwans, A. P., Vasudevan, A., Queener, S. F., Kisliuk, R. L., Cody, V., Li, R., Galitsky, N., Luft, J. R. & Pangborn, W. (1998). *J. Med. Chem.* **41**, 3426–3434.
Hendrickson, W. A. & Konnert, J. H. (1980). *Computing in Crystallography*, edited by R. Diamond, S. Ramaseshan & K. Venkatesen, p. 13.01. Bangalore: Indian Academy of Sciences.
Laskowski, R. A., MacArthur, M. W., Moss, D. S. & Thornton, J. M. (1993). *J. Appl. Cryst.* **26**, 283–291.
Luft, J. R., Rak, D. M. & DeTitta, G. T. (1999*a*). *J. Cryst. Growth*, **196**, 450–455.
Luft, J. R., Rak, D. M. & DeTitta, G. T. (1999*b*). *J. Cryst. Growth*, **196**, 447–449.
Masur, H., Polis, M. A., Tuazon, C. V., Ogota, A. D., Kovacs, J. A., Kaz, D., Hilt, D., Simons, F., Feuerstein, I., Lingren, B., Lane, H. C., Chabner, B. A. & Allegra, C. J. (1993). *J. Infect. Dis.* **167**, 1422–1426.
Mills, J. & Masur, H. (1990). *Sci. Am.*, **263**, 50–57.
Otwinowski, Z. & Minor, W. (1997). *Methods Enzymol.* **276**, 307–326.
Roos, D. S. (1993). *J. Biol. Chem.* **268**, 6269–6280.
Sack, J. S. (1988). *J. Mol. Graph.* **6**, 244–245.
Tripos Inc. (1997) *SYBYL*, version 6.0. Tripos Inc., St Louis, MO, USA.